





Long-Haul mmWave Sky Links: A Multi-Hop NFP-Based Design and Analysis

ABDULLATEEF ALMOHAMAD ¹ (Graduate Student Member, IEEE), **MOHAMAD T. DABIRI**²,
MAZEN O. HASNA ² (Senior Member, IEEE), **TAMER KHATTAB** ² (Senior Member, IEEE),
AND KHALID QARAQE ¹ (Senior Member, IEEE)

¹Department of Electrical and Computer Engineering, Texas A&M University at Qatar, Doha 5825, Qatar

²Department of Electrical Engineering, Qatar University, Doha 2713, Qatar

CORRESPONDING AUTHOR: ABDULLATEEF ALMOHAMAD (e-mail: abdullateef@ieee.org)

This publication was made possible in part by NPRP13S-0130-200200 from the Qatar National Research Fund (a member of The Qatar Foundation) and by the support of Texas A&M at Qatar 2022 research initiatives, open access funding provided by the Qatar National Library. The statements made herein are solely the responsibility of the author[s].

ABSTRACT Networked flying platforms (NFPs) have emerged as a favorable solution to extend the network coverage and/or capacity in temporary scenarios, such as disasters or mega-size events, thanks to their flexibility and cost efficiency. However, in order to provide a reliable multihop link through NFPs, multiple parameters should be considered and optimized, such as the antenna gains, and the number of NFPs required to achieve a certain level of quality of service (QoS). Furthermore, the design of such parameters when considering the hovering fluctuation of NFPs becomes more challenging. In this paper, we study the performance of a long millimeter wave (mmWave) link through multiple NFPs to connect a remote area with the core network taking into account the fluctuation of NFPs. In specific, we derive the outage probability (OP) for such a system under practical considerations, such as NFP fluctuation variance, realistic 3D radiation patterns, gaseous absorption losses, number and distribution of NFPs. Furthermore, we propose a spatial formation for NFPs to reduce interference along the path. Extensive simulations are provided to validate the analytical findings and to reveal insightful trade-offs that help in designing such links.

INDEX TERMS Antenna pattern, backhaul/frounhaul links, mmWave communication, networked flying platforms (NFPs), positioning, unmanned aerial vehicles (UAVs).

I. INTRODUCTION

Many natural disasters such as hurricanes and earthquakes, can knock down traditional terrestrial-based communications, let alone the mega-events with huge number of users gathering in a small area which would congest the network and lead to degraded quality of service (QoS) or service outage. Attempting to address such scenarios, next-generation cellular networks will inevitably rely on two (among others) technologies; high-frequency millimeter wave (mmW) bands and networked flying platforms (NFPs) [1], [2], [3], [4], [5], [6], [7]. The former would keep up with the increasing demand on high data rate, while the latter supports the ubiquity and flexibility requirements of future communication networks [4]. The need for a flexible and cost efficient solution rises up in various scenarios when terrestrial communication

infrastructures fail to provide coverage or sufficient capacity such as natural disasters or temporary events where a small area is overcrowded by users beyond the network capacity and/or coverage. In such events, providing a temporary coverage extension through traditional terrestrial backhauling is time consuming and costly, while deploying NFPs is more cost efficient and can fulfill the timely need of communication for rescue operations or event attendees [5], [8].

A promising combination with aerial backhauling, mmWave band is proposed in [9], since mmWave signals suffer from bad propagation and usually require line-of-sight which makes this band more suitable for aerial communications. Furthermore, the large available bandwidth at mmWave bands makes it favorable for point-to-point backhauling purposes, and although signals in such bands

suffer from high path loss, compact-form highly directional antennas can be mounted on NFPs, thanks to the short wavelength at this band. However, as discussed in the next subsection, high directional antennas have a limitation when mounted on NFPs due to aerodynamic considerations and because of the atmospheric turbulence and fluctuations which makes the realisation of reliable links through NFPs a challenging task.

NFPs as relays can facilitate the fronthaul links between a base station and users in either uplink or downlink direction. Backhauling scenarios can be achieved through relaying over single or multiple NFPs capitalizing on their flexibility, low cost, and favorable channel conditions over terrestrial alternatives. In both scenarios, a relaying protocol can be adopted such as decode-and-forward (DF) and amplify-and-forward (AF). DF schemes have been shown to be superior in performance as compared to AF schemes. However, employing DF relaying involves higher complexity at the NFP's side [10].

A. RELATED WORKS AND CONTRIBUTIONS

The adoption of NFPs in mmWave bands backhauling has been thoroughly studied in the literature [11], [12], [13], [14], [15], [16], [17], [18], while other works [19], [20], [21] have considered the random effects of NFP vibration or atmospheric turbulence for free-space optical (FSO) communication systems, and few works [9], [22], [23] considered the fluctuation effects in mmWave bands for simplified scenarios.

The authors in [11] studied the NFP-assisted backhauling system in mmWave band taking into account the dynamic blockage phenomena in such bands. An analytical framework is provided to study this system in terms of OP and spectral efficiency. However, antenna alignment is assumed perfect in this work which is not practical especially in mmWave and higher frequencies. A similar system is studied in [12] utilizing stochastic geometry to quantify the probability of establishing a backhauling link. The authors in [13] realised a more practical scenario by taking the users mobility into account and optimizing the positions of NFPs that support both backhauling and fronthauling by employing practical 3rd generation partnership project (3GPP) antenna models. As reported, by optimizing the NFPs positions using particle swarm optimization algorithm in a backhaul-aware manner, a gain of about 0.2 Gb/s is obtained in the sum rate for all users. Similarly, in [15], the location of unmanned aerial vehicles (UAVs) and bandwidth allocation are optimized to maximize a modified version of Paris Metro Pricing model. All of these works ignored the NFP fluctuation or turbulence despite their significant effect at mmWave and higher frequencies. Moreover, the effect of fluctuation or pointing errors highly affects the system performance when employing highly directional antennas.

The random fluctuation due to motor or propellers rotation, or atmospheric turbulence has been sufficiently studied in FSO systems. For instance, in [19], the authors studied an FSO link between a high altitude platform (HAP) and UAV hovering at a low altitude, taking into account both the atmospheric turbulence and pointing errors caused by UAV's

hovering. In specific, it is assumed that the transmitter at the HAP transmits an optical beam that has a Gaussian footprint, while the photo-detector at the UAV is supposed to be at the center of the Gaussian beam. However, due to hovering of the UAV, it is shifted randomly causing pointing errors. It is shown that this displacement has a significant effect on OP and outage capacity of the link. A multihop link is studied in [20] where multiple UAVs, acting as relays, provide FSO connectivity between two far apart points while taking into account the orientation fluctuation of UAVs. It is shown that optimizing the beamwidth can alleviate the effects of orientation fluctuation on the outage performance.

Unlike the case of FSO communications, where the fluctuation effect on the link has an almost on-off behaviour, in mmWave bands the orientation fluctuation has a more complex effect on the system performance and it is generally more challenging to study, since it involves the antenna radiation pattern approximations [24]. The authors in [22] employed a robotic arm to emulate the turbulence due to wind gusts affecting UAVs and measured a Doppler spread of about ± 20 Hz at carrier frequency of 28 GHz. The authors in [9], which is among the first works to consider UAV fluctuations in mmWave bands, provided analytical framework to study multiple aerial communication scenarios involving UAV fluctuations. It is shown that high antenna gains are beneficial in low signal-to-noise ratio (SNR) regime while lower gain antennas are more favorable in high SNR regions as a lower gain antenna has a wider beamwidth and thus the fluctuation effects are minimal in this case. This note is further confirmed in [23] by employing square antenna arrays and incorporating fluctuations in two directions. However, in scenarios when the interference is incorporated in the analysis, this note would not be generally correct since wide beamwidth would cause higher levels of interference.

In this paper,¹ motivated by the previous discussion, a long NFP-assisted backhaul link is studied, as shown in Fig. 1(a). In specific, a practical scenario is investigated where inter-NFP interference is incorporated in the analysis while considering the fluctuations which is, to the best of our knowledge, the first time to be addressed in the literature. The OP of this system is studied, where a closed form expression is provided for the end-to-end (E2E) OP. Furthermore, a novel spatial formation for NFPs is proposed and optimized to compensate the inter-NFP interference. In particular, the backhauling link is characterized as a function of the aforementioned parameters and the OP for the E2E link is derived. Analytical findings are verified by Monte Carlo simulations for various parameter sets and scenarios in order to understand the relations between different parameters, to optimize the radiation directivity gain and the spatial formation of NFPs to alleviate the fluctuation effects, and to reveal important design trade-offs in such systems. The main contributions of this paper are summarised as follows

¹This work is an extension of our previous conference paper [24], where we studied a simplified system while ignoring the inter-NFP interference.

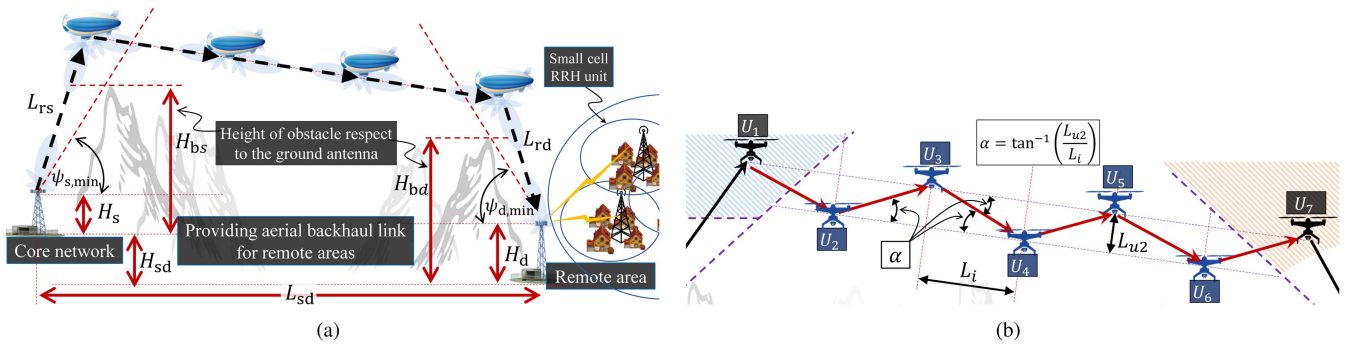


FIGURE 1. System model. (a) A vertical cross-section illustration of a long aerial backhaul link. (b) A top view illustration of NFPs' zigzag pattern.

- Long aerial backhauling system is proposed taking into account the NFPs fluctuations and inter-NFP interference.
- The E2E OP is derived under practical considerations such as antenna radiation patterns, mmWave gaseous absorption model and spatial distribution of NFPs.
- A spatial formation of NFPs is proposed to mitigate inter-NFP interference under such scenarios while taking the NFP fluctuation into account.
- Various scenarios are studied numerically and verified by analysis which revealed important design insights for such systems.

The rest of this paper is organized as follows. We characterize the system and channel models of a long NFP-based mmWave backhaul link in Section II. Then, in Section III, we provide an analytical closed-form expression for OP along with optimal parameter system design highlights. In addition, we propose a spatial formation of NFPs to minimize interference. Next, in Section IV, the performance of long NFP-based mmWave backhaul link is analyzed in terms of OP, and simulation results are presented and discussed. Finally, conclusions are drawn in Section V.

II. THE SYSTEM MODEL

A long mmWave backhauling link is considered as shown in Fig. 1(a), where a multi-hop link is formed through NFPs to render a low cost and flexible solution to provide connectivity to remote areas in case of terrestrial infrastructure failure. Moreover, the considered topology can be used to provide high speed internet connectivity for a remote area as a more affordable alternative in comparison with the fiber networks in order to reduce the costs of trenching fiber optic cables to the remote area. This is even more appealing when the demand is temporary and/or varies substantially in time/location.

Since highly directional antennas are mounted on NFPs, the deployment of NFPs on a straight line will result in a high inter-NFP interference. Hence, we propose a zigzag formation of NFPs in the horizontal plane as shown in Fig. 1(b). As will be shown in the sequel, the zigzag angle α has an optimal value related to the considered other parameters such as the inter-NFP distance and the gain of the directional antennas. The intermediate relays in the multihop link are denoted as U_i for $i \in \{2, \dots, M - 1\}$, where M is the number of NFPs, and

TABLE I The List of Main Notations

Parameter	Description
$q \in \{t, r\}$	This subscript is used to specify Tx and Rx
$w \in \{s, d\}$	This subscript is used to specify A_s and A_d
M	Number of NFPs
U_i	Denote NFP relays for $i \in \{1, \dots, M\}$
$A_{t,i} \& A_{r,i}$	Tx and Rx antennas of U_i
$A_s \& A_d$	Antenna of core network and destination, respectively
$P_{t,s} \& P_{t,i}$	Transmitted power of A_s and A_i for $i \in \{1, \dots, M\}$
$G_s \& G_d$	Pattern gain of A_s and A_d , respectively
$G_{t,i} \& G_{r,i}$	Pattern gain of $A_{t,i} \& A_{r,i}$, respectively
$N_{q,i}$	$N_{q,i} \times N_{q,i}$ is the number of antenna elements of $A_{q,i}$
N_w	is the number of antenna elements of A_w
λ and f_c	Wavelength and carrier frequency
$h_{L_s} \& h_{L_d}$	Channel loss of A_s to $A_{r,1}$ and $A_{t,M}$ to A_d links
$h_{L_{i,j}}$	Channel loss $A_{t,i}$ to $A_{r,j}$ link
$\theta_{tx,i,j} \& \theta_{ty,i,j}$	AoD of $A_{t,i}$ in directions of x and y when observed by $A_{r,j}$
$\theta_{rx,i,j} \& \theta_{ry,i,j}$	AoA of $A_{r,i}$ in directions of x and y when observing $A_{t,j}$
σ_θ^2	Variance of RVs $\theta_{qx,i}$ and $\theta_{qy,i}$ where $q \in \{t, r\}$
$\theta_{pu,i,j}$	Interference angle between $A_{t,i}$ and $A_{r,j}$
α	Zigzag pattern angle
$L_s \& L_d$	Link length of A_s to U_1 and U_M to A_d links
L_i	Horizontal distance between consecutive NFPs
$L_{i,j}$	Length of $A_{t,i}$ to $A_{r,j}$
L_w, ef	$L_w \cos(\psi_w)$
L_{sd}	Horizontal distance between A_s and A_d
L_{u2}	Width of the zigzag pattern

U_1 and U_M respectively represent the first and last NFPs as shown in Fig. 1. The core network transmitter (source) communicates with the first NFP U_1 , where the signal traverses through the intermediate NFPs to reach the last NFP U_M and finally to be forwarded to the destination at the remote area. Each NFP is equipped with two highly directional antennas, one for transmission and the other is for reception. Let us denote the transmitter and receiver antennas at NFP U_i for $i \in \{1, \dots, M\}$ as $A_{t,i}$ and $A_{r,i}$, respectively. Similarly, the core network and destination antennas are denoted as A_s and A_d , respectively. The rest of notations are presented in Table I. We assume that all NFP nodes are equipped with simple

tracking mechanisms to enable them to track the neighbouring NFPs to be aligned with each other. It is worth mentioning that this alignment and tracking is usually coarse and is done by means of control methods benefiting from location information. Therefore, as will be shown in the coming sections, this alignment undergoes fluctuations around the center direction which causes fluctuations in the desired received power and interference level as well. It is assumed that all links are operating at the same frequency band and that each NFP performs DF relaying. It should be stressed here that adopting DF relaying imposes higher complexity at the NFP side while allowing better performance. However, this choice is done in the paper to demonstrate the performance of the multihop system while emphasizing the role of other, more related, parameters as discussed in the following sections. Furthermore, we assume that there is no interference between terrestrial ends (source and destination) and the NFPs, and each NFP can cause interference to the adjacent NFPs only. The received signal-to-interference-plus-noise ratio (SINR) at the first NFP, i -th NFP for $i \in \{2, \dots, M\}$, and destination are obtained respectively as

$$\gamma_{r,1} = \frac{P_{r1}}{N_1}, \quad (1)$$

$$\gamma_{r,i} = \frac{P_{ri}}{I_i + N_i}, \quad (2)$$

$$\gamma_{r,d} = \frac{P_{rd}}{N_d}, \quad (3)$$

with

$$\begin{aligned} P_{r1} &= P_{t,s} h_{L_{s,1}} G_s(\theta_{tx,s,1}, \theta_{ty,s,1}) G_{r,1}(\theta_{rx,1,s}, \theta_{ry,1,s}) \\ P_{ri} &= P_{t,i-1} h_{L_{i-1,i}} G_{t,i-1}(\theta_{tx,i-1,i}, \theta_{ty,i-1,i}) G_{r,i}(\theta_{ry,i,i-1}) \\ P_{rd} &= P_{t,M} h_{L_{M,d}} G_{t,M}(\theta_{tx,M,d}, \theta_{ty,M,d}) G_d(\theta_{rx,d,M}, \theta_{ry,d,M}), \end{aligned} \quad (4)$$

$$I_i = \sum_{k=1}^{i-2} P_{t,k} h_{L_{k,i}} G_{t,k}(\theta'_{ty,k,i}) G_{r,i}(\theta'_{ry,i,k}) \quad (5)$$

where N_1 , N_d and N_i represent the noise power at U_1 , the destination, and U_i , respectively, $P_{t,M}$ is the transmitted power of the last NFP, $P_{t,s}$ and $G_s(\theta_{tx,s,1}, \theta_{ty,s,1})$ are the transmitted power and the antenna gain of the ground transmitter, $P_{t,i}$ and $G_{t,i}(\theta_{ty,i,j})$ are respectively the transmitted power and the antenna gain of $A_{t,i}$, $G_{r,i}(\theta_{ry,i,j})$ is the antenna gain of $A_{r,i}$, and $G_d(\theta_{rx,d,M}, \theta_{ry,d,M})$ is the antenna gain of the ground destination. The parameters $h_{L_{s,i}}$, $h_{L_{i,d}}$, and $h_{L_{i,j}}$ for $i, j \in \{1, \dots, M\}$ respectively denote the channel loss of source to U_i link, U_i to destination link, and U_i to U_j link. The NFPs' vibrations are characterized by random variables $\theta_{ty,i,j}$, $\theta_{ry,i,j}$, $\theta'_{ty,k,i}$, $\theta'_{ry,k,i}$, $\theta_{tx,i,j}$, and $\theta_{rx,i,j}$ which are well defined later in Section II-C.

A. CHANNEL PROPAGATION LOSS

In normal atmospheric conditions, water vapor (H_2O) and oxygen (O_2) molecules are strongly absorptive of radio signals, especially at mmWave frequencies and higher.

The resulting attenuation is in excess of the reduction in radiated signal power due to free-space loss. Channel loss is usually expressed in dB and it can be calculated using the formula

$$h_{L,dB}^{\text{tot}}(f_c) = 20 \log\left(\frac{4\pi L}{\lambda}\right) + h_{L,dB}^{o,w}(f_c), \quad (6)$$

where the first term is the free-space path loss [25], L is the link length (in m), λ is the wavelength (in m), f_c is mmWave frequency (in GHz), $h_{L,dB}^{o,w}(f_c) = \frac{h_{L,dB/km}^{o,w}(f_c)L}{1000}$ is the attenuation due to oxygen and water (in dB), and $h_{L,dB/km}^{o,w}(f_c) = h_{L,dB/km}^o(f_c) + h_{L,dB/km}^w(f_c)$ is the attenuation due to oxygen and water (in dB/km). At 20 °C surface temperature and at sea level, approximate expressions for the attenuation constants of oxygen and water vapor (in dB/km) are provided in an International Telecommunications Union (ITU) report as per [26].

In our system model, inter-NFP links are approximately horizontal, while the links between core to NFPs (CU) and destination to NFPs (DU) are slant where the corresponding models are adopted from [26].

B. ANTENNA PATTERN

Highly directional antennas are required to combat high propagation losses in mmWave bands, and especially in an NFP where power sources are limited. Thanks to the high frequencies in mmWave bands, compact form highly directional antennas can be designed and accommodated on NFPs.

Assuming that the NFPs are distributed over the z -axis between the source and destination, NFPs symmetrically fluctuate in both $x-z$ and $y-z$ axes [23]. However, due to aerodynamic considerations, the intermediate NFPs (U_2, \dots, U_{M-1}) are equipped with a linear array antenna rather than a planar one to enhance stability. Therefore, the radiation pattern is approximately symmetrical in one direction and directional in the other. Hence, without loss of generality, for the inter-NFP links we consider fluctuations around $y-z$ direction only since NFPs are equipped with linear array antennas. However, for the first hop, source to U_1 and last hop, U_M to destination, fluctuations are not considered as we assume that ground ends have accurate mechanisms of tracking, where both the source and the destination, U_1 and U_M , are equipped with a square array antenna with $N \times N$ antenna elements with the same spacing between elements in the x - and y -directions.

The array radiation gain is mainly formulated in the direction of θ and ϕ . In our model, in the first and last hops with planar arrays of antennas, θ and ϕ can be defined as functions of random variables (RVs) θ_x and θ_y as follows

$$\begin{aligned} \theta &= \tan^{-1}\left(\sqrt{\tan^2(\theta_x) + \tan^2(\theta_y)}\right), \\ \phi &= \tan^{-1}(\tan(\theta_y)/\tan(\theta_x)). \end{aligned} \quad (7)$$

By taking into account the effect of all elements, the array radiation gain in the direction of angles θ_x and θ_y will be:

$$G(\theta_x, \theta_y) = G_0(N) G_e(\theta_x, \theta_y) G_a(\theta_x, \theta_y), \quad (8)$$

where G_a is an array factor, G_e is a single element radiation pattern and G_0 is a normalization constant. The 3GPP single element radiation pattern $G_{e,3\text{ dB}} = 10 \times \log_{10}(G_e)$ is adopted from [27]. The array factor $G_a(\theta_x, \theta_y)$ for a uniform excitation amplitude over the square array can be obtained from [28, eqs. (6.89) and (6.91)] as follows

$$G_a(\theta_x, \theta_y) = \left(\frac{\sin\left(\frac{N(kd_x \sin(\theta) \cos(\phi) + \beta_x)}{2}\right)}{N \sin\left(\frac{kd_x \sin(\theta) \cos(\phi) + \beta_x}{2}\right)} \times \frac{\sin\left(\frac{N(kd_y \sin(\theta) \sin(\phi) + \beta_y)}{2}\right)}{N \sin\left(\frac{kd_y \sin(\theta) \sin(\phi) + \beta_y}{2}\right)} \right)^2, \quad (9)$$

where β_x and β_y are progressive phase shift between the elements along the x and y axes, respectively. It is assumed that, without loss of generality, $\beta_x = \beta_y = 0$ and the hovering NFP sets its antenna main-lobe direction on the z axis.

Similarly, the array factor G_a of linear array antennas, used for the intermediate NFPs U_i for $i \in \{2, \dots, M-1\}$, is defined as follows

$$G_a(\theta_y) = \left(\frac{\sin(\pi N \theta_y)}{N \sin(\pi \theta_y)} \right)^2, \quad (10)$$

where θ_y is the random variable representing the angle fluctuations in the y -axis, while fluctuations in x -axis are ignored because of the symmetry of the radiation pattern.

C. THE EFFECT OF NFP'S INSTABILITIES

In practical situations, an error in the mechanical control system of NFPs, mechanical noise, position estimation errors, air pressure, and wind speed can affect the NFP's angular and position instability [29]. The instantaneous orientation of an NFP can randomly deviate from its mean denoted by $\theta_{pu,i,j}$. Let RVs $\theta_{ty,i,j} \sim \mathcal{N}(\theta_{pu,i,j}, \sigma_\theta^2)$ and $\theta_{ry,i,j} \sim \mathcal{N}(\theta_{pu,i,j}, \sigma_\theta^2)$ denote the instantaneous AoD of Tx and AoA of Rx antennas mounted on U_i around the y -axis with respect to the location of U_j . It is worth noting that the mean equals zero ($\theta_{pu,i,j} = 0$) when the nodes U_i and U_j are aligned with each other and the fluctuation happens around the angle $\theta_{pu,i,j} = 0^\circ$ that gives the maximum antenna gain as shown earlier. However, since the interfering NFPs U_k are not aligned with the interfered NFP U_i , thanks to the zigzag pattern, the captured interference power will be scaled by the antenna gains observed from non-zero angle $\theta_{pu,i,k} \neq 0$ where $\theta_{pu,i,k}$ is the interference angle between the i^{th} NFP and the k^{th} interfering NFP. For clarity, we denote the random variables $\theta_{ty,k,i}$ and $\theta_{ry,k,i}$ with non-zero mean $\theta_{pu,i,k} \neq 0$ as $\theta'_{ty,k,i}$ and $\theta'_{ry,k,i}$, respectively.

III. PERFORMANCE ANALYSIS

A. NFPS SPATIAL FORMATION

If the interference effect is neglected, the best performance is obtained by distributing the NFPs over a straight line [24]. However, in case all NFPs operate at the same frequency band, the worst performance occurs when the NFPs are distributed

over a line because of the high inter-NFP interference from the main lobe of antenna radiation patterns. A zigzag formation of terrestrial access point relays has been proposed in [30], and it has been shown that steering the nulls of the radiation pattern of adjacent relays reduces interference and improves the overall system capacity. In this section, we adopt the zigzag formation to mitigate interference while considering the NFPs fluctuation. Specifically, the NFPs are distributed over a zigzag pattern in the horizontal plane as shown in Fig. 1(b), where a non-zero angle α is introduced between interfering NFPs. This formation introduces an extra optimization parameter which is the width of the zigzag pattern L_{u2} . The zigzag angle is varied by changing the width of the zigzag pattern L_{u2} while fixing the inter-NFP horizontal distance L_i as shown in Fig. 1(b). Therefore, the interference angle between the i -th and $(i+k)$ -th NFP, with $k \geq 2$, can be written as

$$\theta_{pu,i,i+k} = \begin{cases} \tan^{-1}\left(\frac{L_{u2}}{L_i}\right), & \text{if } k \text{ is even} \\ \tan^{-1}\left(\frac{L_{u2}}{(k-1)L_i}\right), & \text{if } k \text{ is odd} \end{cases} \quad (11)$$

It should be noted that since the E2E distance L_{sd} is fixed the horizontal distances between NFPs is assumed, without loss of generality, to be equal, i.e., $L_i = \frac{L_{sd}}{M}$.

B. OUTAGE PROBABILITY

The E2E OP \mathbb{P}_{out} is obtained as follows

$$\mathbb{P}_{\text{out}} = 1 - (1 - \mathbb{P}_{\text{out},s1}) (1 - \mathbb{P}_{\text{out},\text{Md}}) \prod_{i=2}^M (1 - \mathbb{P}_{\text{out},i}) \quad (12)$$

where

$$\mathbb{P}_{\text{out},s1} = \sum_{j=1}^{JK} \left(e^{-\frac{2(j-1)^2}{J^2 N_{r,1}^2 \sigma_\theta^2}} - e^{-\frac{2j^2}{J^2 N_{r,1}^2 \sigma_\theta^2}} \right) \times \mathbb{Y}(N_1 \gamma_{r,\text{th}} - P'_{r,1}(j)), \quad (13)$$

$$\mathbb{P}_{\text{out},\text{Md}} = \sum_{j=1}^{JK} \left(e^{-\frac{2(j-1)^2}{J^2 N_{t,M}^2 \sigma_\theta^2}} - e^{-\frac{2j^2}{J^2 N_{t,M}^2 \sigma_\theta^2}} \right) \times \mathbb{Y}(N_d \gamma_{r,\text{th}} - P'_{r,d}(j)), \quad (14)$$

$$\mathbb{P}_{\text{out},i} = 1 - \sum_{j_1=1}^{KJ} \dots \sum_{j_M=1}^{KJ} \mathcal{A}_{j_1, j_2, \dots, j_M} \left[\mathcal{Q}\left(\frac{2(j_1-1)}{JN_{t,i-1}\sigma_\theta}\right) - \mathcal{Q}\left(\frac{2j_1}{JN_{t,i-1}\sigma_\theta}\right) \right] \times \left[\mathcal{Q}\left(\frac{2(j_2-1)}{JN_{r,i}\sigma_\theta}\right) - \mathcal{Q}\left(\frac{2j_2}{JN_{r,i}\sigma_\theta}\right) \right] \times \prod_{m=3}^M \left[\mathcal{Q}\left(\frac{2(j_m-1)}{JN_{t,i-m+1}\sigma_\theta}\right) - \mathcal{Q}\left(\frac{2j_m}{JN_{t,i-m+1}\sigma_\theta}\right) \right] \quad (15)$$

and $\mathbb{Y}(x)$ is the sign function. Also, the parameters $P'_{r,1}(j)$ and $\mathcal{A}_{j_1, j_2, \dots, j_M}$ are defined in (22) and (35), respectively. For the proof, please refer to Appendix A.

The OP expression given in (15) is intuitive since we have approximated the radiation pattern by adopting its sampled counterpart. The coverage event happens when the transmitter and receiver antennas are experiencing some rotation angles with probabilities $\left[Q\left(\frac{2(j_1-1)}{JN_{r,i-1}\sigma_\theta}\right) - Q\left(\frac{2j_1}{JN_{r,i-1}\sigma_\theta}\right) \right]$ and $\left[Q\left(\frac{2(j_2-1)}{JN_{r,i}\sigma_\theta}\right) - Q\left(\frac{2j_2}{JN_{r,i}\sigma_\theta}\right) \right]$, respectively. The interference resulting from the configuration of the interfering nodes with probability $\prod_{m=3}^M \left[Q\left(\frac{2(j_m-1)}{JN_{r,i-m+1}\sigma_\theta}\right) - Q\left(\frac{2j_m}{JN_{r,i-m+1}\sigma_\theta}\right) \right]$, which makes the SINR larger than the said threshold $\gamma_{r,\text{th}}$. Therefore, the indicator function $\mathcal{A}_{j_1, j_2, \dots, j_M}$ takes value 1 to add up the probability of the given configurations of all involved antennas as a coverage event probability.

Furthermore, it can be easily verified that the OP tends to 1 when the number of NFPs $M \rightarrow \infty$ which is confirmed by numerical simulations. This can be verified by noticing that the E2E distance is fixed (or at least finite), therefore, by increasing the number of NFPs to infinity, the link will be overcrowded by NFPs and the interference will overwhelm the desired signal. Furthermore, as the number of antenna elements increases $N \rightarrow \infty$, the OP tends to 1 which is also confirmed by simulations, and it is because the radiation beamwidth will tend to 0 (very narrow beam) and hence the SNR becomes 0 as well.

In the next section, by providing sufficient simulations for conventional values of the channel parameters at 70 GHz, we will show that by incorporating the interference in the system, the worst case scenario is when the NFPs are distributed over a straight line which was the optimal scenario when ignoring the interference [24]. Due to page limitations, optimal system design under frequency reuse is out of the scope of this work, and is left for future consideration. However, we will show the effect of spatial formation of NFPs to reduce interference in case all NFPs operate at the same frequency bands.

C. SPECIAL CASE: WITHOUT INTERFERENCE

In case the interference between NFPs is neglected, as in [24], the optimal spatial formation of NFPs will be a straight line. Therefore, the OP can be easily obtained for the first and last hops by setting $N_1\gamma_{\text{th}} = P_{r,\text{th}}$ and $N_d\gamma_{\text{th}} = P_{r,\text{th}}$ in (13) and (14), respectively. The outage of the inter-NFP links is derived in a similar way as follows

$$\mathbb{P}_{\text{out},i} = \sum_{j=1}^{JK} \sum_{j'=1}^{JK} \left(e^{-\frac{2(j-1)^2}{J^2 N_{r,i-1}^2 \sigma_\theta^2}} - e^{-\frac{2j^2}{J^2 N_{r,i-1}^2 \sigma_\theta^2}} \right) \left(e^{-\frac{2(j'-1)^2}{J^2 N_{r,i}^2 \sigma_\theta^2}} - e^{-\frac{2j'^2}{J^2 N_{r,i}^2 \sigma_\theta^2}} \right) \mathbb{Y}(P_{r,\text{th}} - P'_{r,i}(j, j')). \quad (16)$$

TABLE II Parameter Values for Simulations

Parameters	Values	Parameters	Values
$P_{t,s}$	1 W	$P_{t,i}$	200 mW
$N_{q,i}$	4-18	N_w	16
f_c	70 GHz	σ_θ^2	$1^\circ - 4^\circ$
ρ_0	7.5 g/m ³	$\mathbb{P}_{\text{out,tr}}$	10^{-3}
H_{bd}	1 km	$H_{b,\text{max}}$	2 km
$\psi_{d,\text{min}}$	20°	L_{sd}	40 km
T	20°C	$\psi_{s,\text{min}}$	40°

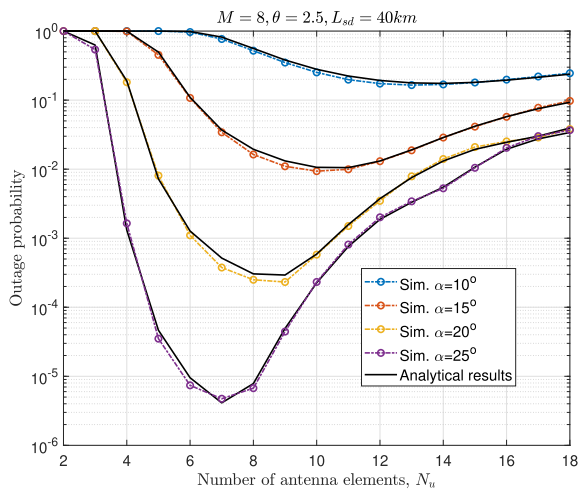
IV. SIMULATION RESULTS

In this section, we first examine the effect of important parameters such as link length, intensity of NFPs' vibrations, antenna pattern, NFP height, frequency band, etc. on the performance of the considered system. Then, using the obtained results, we study the optimal design of the tuneable parameters. The values of the parameters used in the simulations are listed in Table 2. It is worth noting here that the analytical results from (15) are generated by including five interfering NFPs only for the sake of simplicity, and as shown in the figures, this approximation has a good matching with simulation results.

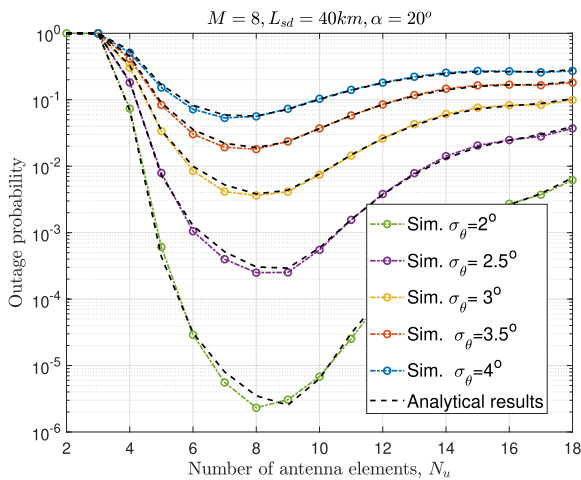
In Fig. 2(a) and (b), E2E OP of a backhauling link is depicted versus the number of antenna elements $N_{t,i} = N_{r,i} = N_u$ for different zigzag angles $\alpha = \{10, 15, 20, 25\}^\circ$ and fluctuation variances $\sigma_\theta = \{2, 2.5, 3, 3.5, 4\}^\circ$, respectively.

In both figures, we fix the E2E distance $L_{sd} = 40$ km and the number of NFPs $M = 8$. We first notice that the analytical approximation of OP has an acceptable matching with numerical simulation results. In Fig. 2(a), the OP improves by increasing the zigzag angle because it makes the captured interference at the interfered NFP arrives from a large angle, i.e. non-zero angle, thus it reduces the inter-NFP interference. Although, increasing the zigzag angle results in shorter interference paths, the non-zero reception angle at the receiving antenna compensates the decreased path loss. Additionally, it is noticed that there is an optimal range for the number of antenna elements. For instance, when the zigzag angle is small, i.e., $\alpha = 10^\circ$, increasing the number of elements N_u generally slightly improves the performance. However, due to the small zigzag angle, the OP is high due to the high captured interference. On the other hand, for larger zigzag angles, there is a shorter range for optimal performance. For instance, when $\alpha = 25^\circ$, $N_u = 6, 8$ gives the lowest OP and using any other number of antenna elements significantly degrades the performance.

In Fig. 2(b), we fix the zigzag angle at $\alpha = 20^\circ$ and analyze the effect of NFP fluctuation standard deviation σ_θ on the OP. As expected, higher σ_θ values results in performance degradation, and the degradation exhibits a diminishing behaviour. Furthermore, the fluctuation standard deviation does not affect the optimal number of antenna elements which stays roughly around $N_u = 8$. In Fig. 3, the E2E OP is plotted versus the



(a)



(b)

FIGURE 2. E2E outage probability versus number of antenna elements N_u when $H_u = 2.5$ km, for (a) different values of zigzag angles α and $\sigma_\theta = 2.5^\circ$, and (b) different values of NFP fluctuation σ_θ with $\alpha = 20^\circ$.

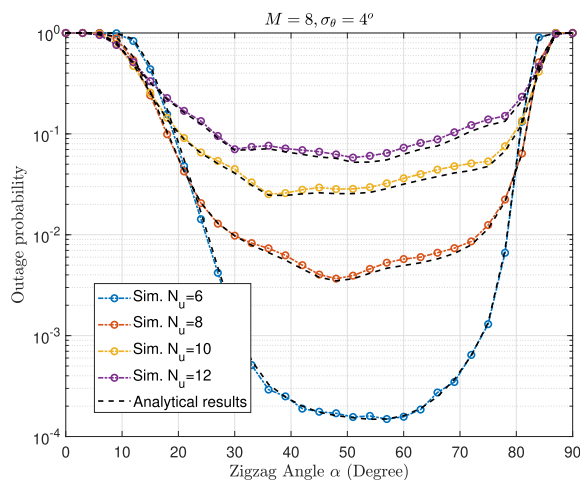


FIGURE 3. E2E outage probability versus zigzag angle with different number of antenna elements $N_u = 6, 8, 10, 12$.

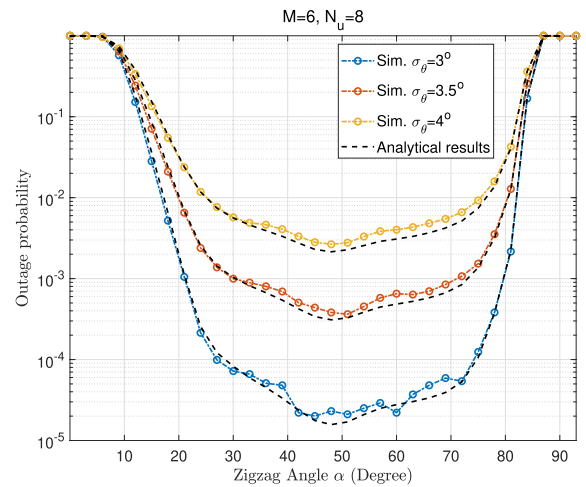


FIGURE 4. Outage probability of inter-NFP links versus zigzag angle and number of NFPs.

zigzag angle with $H_u = 2.5$ km and $\sigma_\theta = 4^\circ$ for four different number of antenna elements, namely $N_u = 6, 8, 10$ and 12 . As noticed in the previous two figures, the higher the number of elements, i.e., the narrower the beamwidth, the smaller the required zigzag angle to achieve the optimal performance. This is due to the fact that since the inter-NFP distance is fixed, increasing the zigzag angle means increasing the vertical distance and hence the inter-NFP distance increases. Therefore, the alignment errors for a narrow beamwidth antenna have significant effects on performance in contrast to wider beamwidth antenna. In addition, according to the adopted radiation pattern, the wider the beamwidth, the lower the antenna gain, and therefore less interference is caused due to misalignment.

The OP is plotted versus the zigzag angle for different fluctuation standard deviations $\sigma_\theta = \{3, 3.5, 4\}^\circ$ in Fig. 4. As seen in previous figures, larger fluctuation variance generally results in worse performance due to high interference caused by misalignment. However, in this scenario, since the number of antenna elements is fixed at $N_u = 8$, changing the fluctuation variance does not affect the optimal zigzag angle which is around $\alpha = 47^\circ$.

In Fig. 5, the E2E OP is plotted versus the E2E horizontal distance L_{sd} for different number of antenna elements and number of NFPs, with zigzag angle $\alpha = 45^\circ$, fluctuation standard deviation $\sigma_\theta = 4^\circ$ and $M = \{5, 8\}$. As expected, increasing the distance L_{sd} results in a higher OP in general. Furthermore, in short distances, the lower number of antenna elements gives the best outage performance. This is because, in short distances, the low antenna gain is sufficient to deliver enough useful power and less interference on the next NFPs, and at the same time it is less sensitive to fluctuations. On the other hand, for larger distances, a higher number of antenna elements results in a better performance which is mainly because of the needed high antenna gain that is required to mitigate the high path loss. Moreover, by comparing the case

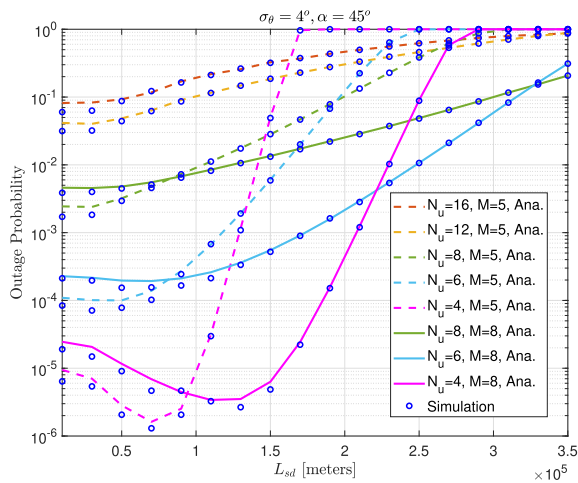


FIGURE 5. E2E outage probability versus E2E distance L_{sd} with different number of antenna elements $N_u = 16, 12, 8, 6, 4$ for $M = \{5, 8\}$, $\sigma_\theta = 4^\circ$ and $\alpha = 45^\circ$.

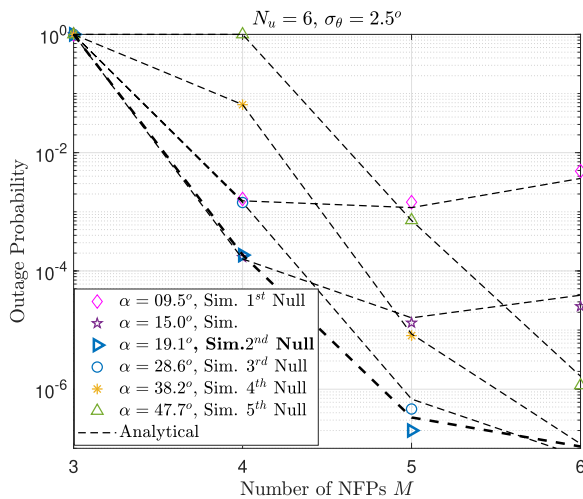


FIGURE 6. E2E outage probability versus number of NFPs M with different zigzag angles $\alpha = \{10, 15, 19.1, 28.6, 38.2, 47.7\}^\circ$ with $N_u = 6$ and $\sigma_\theta = 2.5^\circ$.

with $M = 5$ NFPs and those with $M = 8$ NFPs, dashed and solid lines, respectively, the higher the number of deployed NFPs, the larger distance the link can afford. For instance, by observing the case of $N_u = 4$ for both dashed and solid curves, with $M = 5$ NFPs, the link can reach $L_{sd} = 130$ km with OP less than 10^{-3} while by increasing the number of NFPs to $M = 8$, it can reach 200 km without exceeding the same outage threshold.

Another interesting aspect, inspired by [30], is presented in Fig. 6, where the outage performance is assessed with zigzag angles corresponding to the nulls of the radiation pattern with $N_u = 6$ versus the number of NFPs $M = \{3, 4, 5, 6\}$ and an E2E distance of $L_{sd} = 200$ km. It is noticed that the optimal zigzag angle is the one that corresponds to the second null of the radiation pattern over the considered range of number of NFPs. However, since the E2E distance is fixed, increasing

the number of NFPs would increase the level of inter-NFP interference and leads to higher OP for any zigzag angle. Moreover, there is an optimal number of NFPs for each zigzag angle, i.e. for each null of the radiation pattern, where the nulls with small angles are more suitable for smaller number of NFPs. The larger the null angle, the larger the number of NFPs it can handle before the outage performance starts degrading again. However, in [30], the authors adopt the beam-nulling technique, where an extra null in a certain direction (in our case this would be the direction of interfering with the following NFPs) is introduced to the radiation pattern, by employing beamforming. Beam-nulling, by design, tries to maintain the main-lobe characteristics as close as possible to the original beam pattern; hence, when applied to our configuration, it reduces the inter-NFP interference while maintaining the desired signal almost as is [31]. Therefore, our results in this work, without using beam-nulling, can be considered a lower bound on the performance of a similar configuration that utilizes beam-nulling.

As mentioned earlier, the cost of implementing such a backhaul link is almost proportional to the number of NFPs, M . To reach a better view, in Fig. 7(a) and (b) we analyze the effect of M on the OP of the E2E link for $f_c = 70$ GHz, $L_{sd} = 40$ km and $\sigma_\theta = 3.5^\circ$ with zigzag angles $\alpha = 10^\circ$ and $\alpha = 20^\circ$, respectively.

A better outage performance is noticed with smaller number of NFPs, however, the improvement of the outage performance exhibits a diminishing behaviour as we decrease the number of NFPs. Furthermore, the optimal number of NFPs depends on the number of antennas mounted on the NFPs and the zigzag angle. Another interesting insight from the figures: a lower number of antenna elements is required when the zigzag angle is large for the same number of NFPs to achieve the same OP. From these figures, the maximum required number of NFPs is $M = 4$ to guarantee $\mathbb{P}_{out} < 10^{-3}$ in the considered 40 km distance between the core network and the remote area when zigzag angle is $\alpha = 20^\circ$. For a zigzag angle of $\alpha = 10^\circ$, this outage threshold can not be achieved. A better outage performance is expected by increasing the number of NFPs, which is the opposite of what is noticed in figures Fig. 7(a) and (b). However, by noticing Fig. 5, at small E2E distance, for instance $L_{sd} = 50$ km, adding more NFPs is harmful because of the increased introduced interference. At larger distances, for instance $L_{sd} = 150$ km, increasing the number of NFPs does improve the outage performance, as expected. This is simply because at larger distances, more NFPs are required to compensate the large path losses without inducing significant interference. Moreover, each E2E distance has an optimal number of NFPs, where deploying more NFPs starts degrading the performance because of increased interference levels as confirmed in Fig. 8.

V. CONCLUSION

A performance study of long multihop backhauling links through NFPs is studied in terms of OP considering the NFP

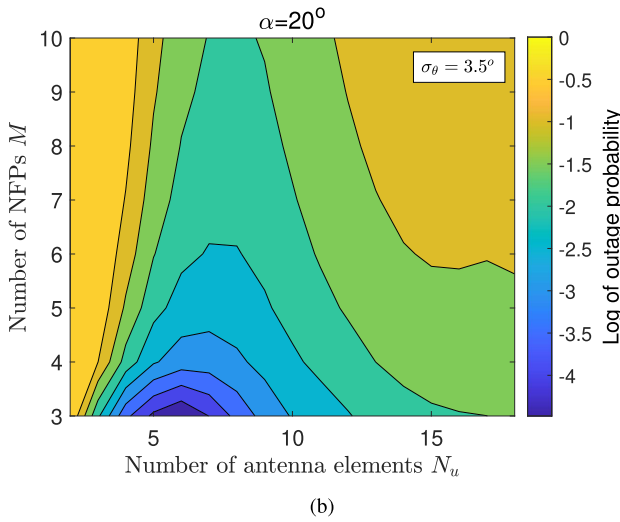
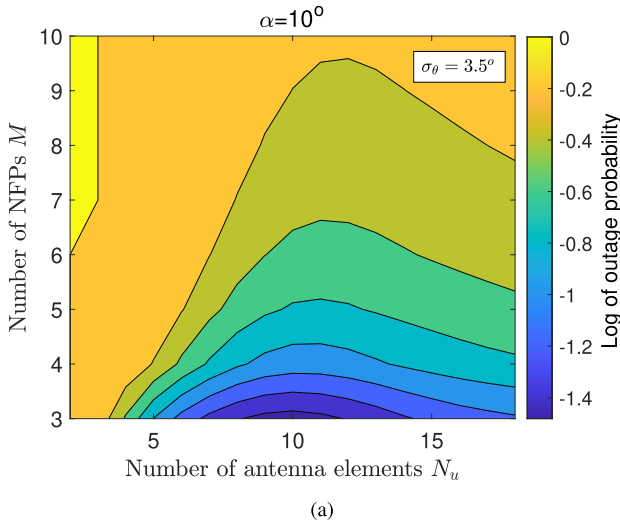


FIGURE 7. E2E outage probability versus number of antenna elements N_u and number of NFPs M when $H_u = 2.5$ km and $L_{sd} = 40$ km, for (a) zigzag angle $\alpha = 10^\circ$, and (b) zigzag angle $\alpha = 20^\circ$.

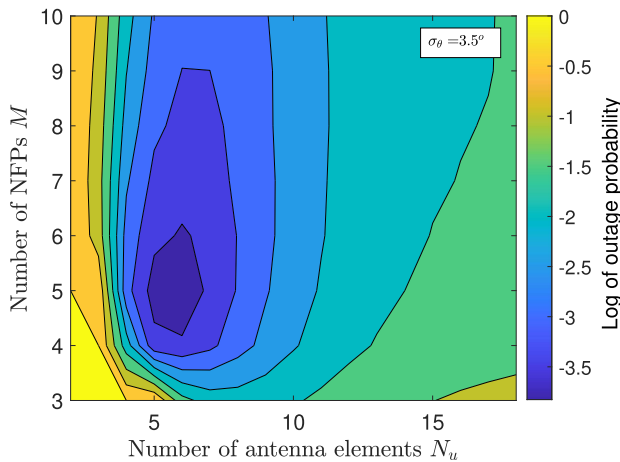


FIGURE 8. E2E outage probability versus number of antenna elements N_u and number of NFPs M when $H_u = 2.5$ km, $L_{sd} = 150$ km and zigzag angle $\alpha = 20^\circ$.

random fluctuations, with a practical antenna radiation pattern and path loss due to gaseous absorption. Additionally, a spatial zigzag formation is proposed for NFPs in order to reduce the inter-NFP interference. Extensive simulation results are provided to show the quality of the derived formulas and reveal some insightful design guidelines for such systems. As future extensions, the inter-NFP horizontal distance can be a variable and optimized for each hop individually, the same can be done for the number of antenna elements at each NFP.

APPENDIX A

For the considered multihop DF relaying system, the OP of the E2E system is given by [32]

$$\mathbb{P}_{\text{out}} = 1 - (1 - \mathbb{P}_{\text{out},s1}) (1 - \mathbb{P}_{\text{out},Md}) \prod_{i=2}^M (1 - \mathbb{P}_{\text{out},i}), \quad (17)$$

where $\mathbb{P}_{\text{out},s1}$, $\mathbb{P}_{\text{out},Md}$, and $\mathbb{P}_{\text{out},i}$ denote the OP of A_s to $A_{r,1}$ link, $A_{t,M}$ to A_d link, and $A_{t,i-1}$ to $A_{r,i}$ link, respectively, and $\gamma_{r,\text{th}}$ is the received SINR threshold. Considering the approximate symmetry of the antenna pattern along the ψ axis, (8) can be approximated as

$$G(\theta_{q_i}) = G_0(N_{q,i}) 10^{\frac{G_{\text{max}}}{10}} \left(\frac{\sin\left(\frac{N_{q,i} k d_x \sin(\theta_{q_i})}{2}\right)}{N_{q,i} \sin\left(\frac{k d_x \sin(\theta_{q_i})}{2}\right)} \right)^2, \quad (18)$$

where $q \in t, r$, $\theta_{q_i} = \sqrt{\theta_{q_x i}^2 + \theta_{q_y i}^2}$. Since RVs $\theta_{q_x i}$ and $\theta_{q_y i}$ have non-zero mean Gaussian distributions, the random variable θ_{q_i} follows the Rician distribution as

$$f_{\theta_{q_i}}(\theta_{q_i}) = \frac{\theta_{q_i}}{\sigma_\theta^2} \exp\left(-\frac{\theta_{q_i}^2 + \mu^2}{2\sigma_\theta^2}\right) \mathcal{I}_0\left(\frac{\mu\theta_{q_i}}{\sigma_\theta^2}\right), \quad (19)$$

where $\mathcal{I}_0(\cdot)$ is the zero order modified Bessel function of the first kind, and $\mu = \sqrt{\mu_{q_x i}^2 + \mu_{q_y i}^2}$. Let us approximate (18) as

$$G(\theta_{q_i}) \simeq G_0(N_{q,i}) 10^{\frac{G_{\text{max}}}{10}} \sum_{j=1}^{KJ} \mathbb{G}(j, N_{q,i}) \left[\mathbb{Y}\left(\theta_{q,i} - \frac{2(j-1)}{JN_{q,i}}\right) - \mathbb{Y}\left(\theta_{q,i} - \frac{2j}{JN_{q,i}}\right) \right], \quad (20)$$

where $\mathbb{G}(j, N_{q,i}) = \left(\frac{\sin\left(\frac{N_{q,i} k d_x \sin\left(\frac{2j}{JN_{q,i}}\right)}{2}\right)}{N_{q,i} \sin\left(\frac{k d_x \sin\left(\frac{2j}{JN_{q,i}}\right)}{2}\right)} \right)^2$, $\mathbb{Y}(x)$ is the

unit step function, and the parameters J and K are the natural numbers that for large values of J , (20) tends to (18). Also, $K = 1$ refers to the main lobe of the antenna pattern and $K > 1$ refers to the number of sidelobes. Note that the problem of orientation fluctuations is related to the antennas mounted on the NFPs. For the ground antennas A_s and A_d , it

is assumed that the ground station does not face weight and power limitations and uses a stabilizer with high accuracy and response speed to track the first and last NFPs. Based on this assumption, and using (1), (19), and (20), the distribution of the received signal power at the A_1 can be derived as

$$f_{P_{r,1}}(P_{r,1}) = \sum_{j=1}^{JK} \left(e^{-\frac{2(j-1)^2}{J^2 N_{q,i}^2 \sigma_\theta^2}} - e^{-\frac{2j^2}{J^2 N_{q,i}^2 \sigma_\theta^2}} \right) \times \delta(P_{r,1} - P'_{r,1}(j)), \quad (21)$$

where $\delta(\cdot)$ is the Dirac delta distribution and

$$P'_{r,1}(j) = P_{t,s} h_{L_s}(\psi_s, L_s) G_0(N_{r,1}) G_0(N_s) \times N_s^2 10^{\frac{G_{\max}}{5}} \mathbb{G}(j, N_{q,i}). \quad (22)$$

Finally, using (21), the OP of A_s to A_1 link can be obtained as in (13). Similarly, by substituting the parameters $N_{t,M}$, N_d , $h_{L_d}(\psi_d, L_d)$, and $P_{t,M}$ instead of the parameters $N_{r,1}$, N_s , $h_{L_s}(\psi_s, L_s)$, and $P_{t,s}$ in (13), respectively, the OP of A_M to A_d link is obtained in (14).

From (2) and (20), the received power at the i^{th} NFP is written as

$$P_{r,i} \simeq P_{t,i-1} h_{L_{i-1}} G_0(N_{t,i-1}) G_0(N_{r,i}) 10^{\frac{G_{\max}}{5}} \times \sum_{j=1}^{KJ} \sum_{j'=1}^{KJ} \mathbb{G}(j, N_{t,i-1}) \mathbb{G}(j', N_{r,i}) \left[\mathbb{Y} \left(\theta_{t,i-1} - \frac{2(j-1)}{JN_{t,i-1}} \right) - \mathbb{Y} \left(\theta_{t,i-1} - \frac{2j}{JN_{t,i-1}} \right) \right] \times \left[\mathbb{Y} \left(\theta_{r,i} - \frac{2(j'-1)}{JN_{r,i}} \right) - \mathbb{Y} \left(\theta_{r,i} - \frac{2j'}{JN_{r,i}} \right) \right]. \quad (23)$$

As we can see, $P_{r,i}$ is a function of two independent RVs $\theta_{t,i-1}$ and $\theta_{r,i}$. Since we assumed that the antennas of the consecutive NFPs are aligned and we neglected fluctuations in the x direction, $\theta_{r,i}$ and $\theta_{t,i}$ for $i \in \{2, 3, \dots, M-1\}$ follow the Gaussian distribution with zero mean. Therefore, from (23) and using [33], and after some manipulations, the PDF of $P_{r,i}$ is derived as

$$f_{P_{r,i}}(P_{r,i}) = \sum_{j=1}^{JK} \sum_{j'=1}^{JK} \left(F_{\theta_t} \left(\frac{2(j-1)}{JN_{t,i-1}} \right) - F_{\theta_t} \left(\frac{2j}{JN_{t,i-1}} \right) \right) \times \left(F_{\theta_r} \left(\frac{2(j'-1)}{JN_{r,i-1}} \right) - F_{\theta_r} \left(\frac{2j'}{JN_{r,i-1}} \right) \right) \delta(P_{r,i} - P'_{r,i}(j, j')), \quad (24)$$

where

$$P'_{r,i}(j, j') = P_{t,i-1} L_{i-1,i} G_0(N_{t,i-1}) G_0(N_{r,i}) 10^{\frac{G_{\max}}{5}} \times \mathbb{G}(j, N_{t,i-1}) \mathbb{G}(j', N_{r,i}), \quad (25)$$

$L_{i,j}$ is the link length between the i^{th} and j^{th} NFPs and $F_{\theta_t}(\cdot)$ is the CDF of random variable θ_t which follows a zero-mean

Gaussian for both θ_t and θ_r . Accordingly, the CDF is written as follows

$$F_{P_{r,i}}(P_{r,i}) = \sum_{j=1}^{JK} \sum_{j'=1}^{JK} A_{j,j'} \mathcal{H}(P_{r,i} - P'_{r,i}(j, j')), \quad (26)$$

where $\mathcal{H}(\cdot)$ denotes the Heaviside Theta function and

$$A_{j,j'} = \left(F_{\theta_t} \left(\frac{2(j-1)}{JN_{t,i-1}} \right) - F_{\theta_t} \left(\frac{2j}{JN_{t,i-1}} \right) \right) \times \left(F_{\theta_r} \left(\frac{2(j'-1)}{JN_{r,i-1}} \right) - F_{\theta_r} \left(\frac{2j'}{JN_{r,i-1}} \right) \right), \quad (27)$$

and the SINR is written as

$$\gamma_{r,i}(\theta_{ty,i-1,i}, \theta_{ry,i,i-1}, \theta'_{ty,k,i}, \theta'_{ry,k,i}) = \frac{P_{r,i}(\theta_{ty,i-1,i}, \theta_{ry,i,i-1})}{I_i(\theta'_{ty,k,i}, \theta'_{ry,k,i}) + N_i} \quad (28)$$

From (28), the SINR $\gamma_{r,i}$ is a functions of RVs $\theta_{ty,i-1,i}$, $\theta_{ry,i,i-1}$, $\theta'_{ty,k,i}$, and $\theta'_{ry,k,i}$ for $k \in \{1, \dots, i-2\}$. Therefore, deriving a closed-form expression for the PDF of $\gamma_{r,i}$ is very difficult if not impossible. Since the effect of interference decreases with increasing distance, then $\gamma_{r,i}$ can be well approximated by incorporating two previous interferers only as follows

$$\gamma_{r,i}(\theta_{ty,i-1,i}, \theta_{ry,i,i-1}, \theta'_{ty,i-2,i}, \theta'_{ry,i-2,i}) = \frac{P_{r,i}(\theta_{ty,i-1,i}, \theta_{ry,i,i-1})}{I'_{i,i-2}(\theta'_{ty,i-2,i}, \theta'_{ry,i-2,i}) + I'_{i,i-3}(\theta'_{ty,i-3,i}, \theta'_{ry,i-3,i}) + I''_i + N_i} \quad (29)$$

where $\theta'_{ty,i-2,i} = \theta_{ty,i-2,i}$

$$I''_i = \sum_{k=1}^{i-3} P_{t,k} L_{k,i} G_{t,k}(\bar{\theta}_{ty,k,i}) G_{r,i}(\bar{\theta}_{ry,k,i}). \quad (30)$$

In (30), the parameters $\bar{\theta}_{ty,k,i}$ and $\bar{\theta}_{ry,k,i}$ are average values of RVs $\theta_{ty,k,i}$ and $\theta_{ry,k,i}$. Since we have $\theta'_{ry,k,i} = \theta_{ry,i,i-1} + \theta_{pu}$, and by using (23) and (25), (29) can be rewritten as (31), shown at the top of the next page. In (31), the parameter $\theta'_{pu} = \tan^{-1}(\frac{L_{pu}}{3L_{pu}^1})$ is the average of antenna angle offset between U_i and U_{i-3} . Also we have

$$P''_{r,i,k}(j, j', \theta_{pu}) = P_{t,k} L_{k,i} G_0(N_{t,k}) G_0(N_{r,i}) 10^{\frac{G_{\max}}{5}} \times \mathbb{G}(j, N_{t,k}, \theta_{pu}) \mathbb{G}(j', N_{r,i}, \theta_{pu}), \quad (32)$$

where

$$\mathbb{G}(j, N_{q,i}, \theta) = \left(\frac{\sin \left(\frac{N_{q,i} k d_x \sin \left(\frac{2j}{JN_{q,i}} + \theta \right)}{2} \right)}{N_{q,i} \sin \left(\frac{k d_x \sin \left(\frac{2j}{JN_{q,i}} + \theta \right)}{2} \right)} \right)^2. \quad (33)$$

$$\begin{aligned} \gamma_{r,i}(\theta_{ty,i-2}, \theta_{ty,i-1}, \theta_{ry,i}) &\simeq \sum_{j_1=1}^{KJ} \sum_{j_2=1}^{KJ} \sum_{j_3=1}^{KJ} \sum_{j_4=1}^{KJ} \frac{P'_{r,i,i-1}(j_1, j_2)}{P''_{r,i,i-2}(j_3, j_2, \theta_{pu}) + P''_{r,i,i-3}(j_4, j_2, \theta'_{pu}) + I'_i + N_i} \\ &\left[\mathbb{Y} \left(\theta_{ty,i-1} - \frac{2(j_1-1)}{JN_{t,i-1}} \right) - \mathbb{Y} \left(\theta_{ty,i-1} - \frac{2j_1}{JN_{t,i-1}} \right) \right] \left[\mathbb{Y} \left(\theta_{ry,i} - \frac{2(j_2-1)}{JN_{r,i}} \right) - \mathbb{Y} \left(\theta_{ry,i} - \frac{2j_2}{JN_{r,i}} \right) \right] \\ &\left[\mathbb{Y} \left(\theta_{ty,i-2} - \frac{2(j_3-1)}{JN_{t,i-2}} \right) - \mathbb{Y} \left(\theta_{ty,i-2} - \frac{2j_3}{JN_{t,i-2}} \right) \right] \left[\mathbb{Y} \left(\theta_{ty,i-3} - \frac{2(j_4-1)}{JN_{t,i-3}} \right) - \mathbb{Y} \left(\theta_{ty,i-3} - \frac{2j_4}{JN_{t,i-3}} \right) \right] \end{aligned} \quad (31)$$

Now, by generalizing (31) to account for all previous interferers, OP of the i th NFP node is obtained as

$$\begin{aligned} \mathbb{P}_{\text{out},i} &= 1 - \sum_{j_1=1}^{KJ} \cdots \sum_{j_M=1}^{KJ} \mathcal{A}_{j_1, j_2, \dots, j_M} \\ &\times \left[Q \left(\frac{2(j_1-1)}{JN_{t,i-1}\sigma_\theta} \right) - Q \left(\frac{2j_1}{JN_{t,i-1}\sigma_\theta} \right) \right] \\ &\times \left[Q \left(\frac{2(j_2-1)}{JN_{r,i}\sigma_\theta} \right) - Q \left(\frac{2j_2}{JN_{r,i}\sigma_\theta} \right) \right] \\ &\times \prod_{m=3}^M \left[Q \left(\frac{2(j_m-1)}{JN_{t,i-m+1}\sigma_\theta} \right) - Q \left(\frac{2j_m}{JN_{t,i-m+1}\sigma_\theta} \right) \right] \end{aligned} \quad (34)$$

where

$$\mathcal{A}_{j_1, j_2, \dots, j_M} = \begin{cases} 1, & \frac{P'_{r,i,i-1}(j_1, j_2)}{\sum_{m=3}^M P''_{r,i,i-m+1}(j_m, j_2, \theta_{pu_m}) + N_i} \geq \gamma_{r,\text{th}} \\ 0, & \text{Otherwise.} \end{cases} \quad (35)$$

REFERENCES

- [1] W. Saad, M. Bennis, and M. Chen, "A vision of 6G wireless systems: Applications, trends, technologies, and open research problems," *IEEE Netw.*, vol. 34, no. 3, pp. 134–142, May/June 2020.
- [2] M. Chen, M. Mozaffari, W. Saad, C. Yin, M. Debbah, and C. S. Hong, "Caching in the sky: Proactive deployment of cache-enabled unmanned aerial vehicles for optimized quality-of-experience," *IEEE J. Sel. Areas Commun.*, vol. 35, no. 5, pp. 1046–1061, May 2017.
- [3] M. Mozaffari, W. Saad, M. Bennis, and M. Debbah, "Mobile unmanned aerial vehicles (UAVs) for energy-efficient Internet of Things communications," *IEEE Trans. Wireless Commun.*, vol. 16, no. 11, pp. 7574–7589, Nov. 2017.
- [4] M. Mozaffari, W. Saad, M. Bennis, Y.-H. Nam, and M. Debbah, "A tutorial on UAVs for wireless networks: Applications, challenges, and open problems," *IEEE Commun. Surv. Tut.*, vol. 21, no. 3, pp. 2334–2360, Jul.–Sep. 2019.
- [5] W. Khawaja, I. Guvenc, D. W. Matolak, U.-C. Fiebig, and N. Schneckenberger, "A survey of air-to-ground propagation channel modeling for unmanned aerial vehicles," *IEEE Commun. Surv. Tut.*, vol. 21, no. 3, pp. 2361–2391, Jul.–Sep. 2019.
- [6] X. Cao, P. Yang, M. Alzenad, X. Xi, D. Wu, and H. Yanikomeroglu, "Airborne communication networks: A survey," *IEEE J. Sel. Areas Commun.*, vol. 36, no. 9, pp. 1907–1926, Sep. 2018.
- [7] R. Amer, W. Saad, and N. Marchetti, "Mobility in the sky: Performance and mobility analysis for cellular-connected UAVs," *IEEE Trans. Commun.*, vol. 68, no. 5, pp. 3229–3246, May 2020.
- [8] M. Alzenad, M. Z. Shaker, H. Yanikomeroglu, and M.-S. Alouini, "FSO-based vertical backhaul/fronthaul framework for 5G+ wireless networks," *IEEE Commun. Mag.*, vol. 56, no. 1, pp. 218–224, Jan. 2018.
- [9] M. T. Dabiri, H. Safi, S. Parsaeefard, and W. Saad, "Analytical channel models for millimeter wave UAV networks under hovering fluctuations," *IEEE Trans. Wireless Commun.*, vol. 19, no. 4, pp. 2868–2883, Apr. 2020.
- [10] Y. Chen, N. Zhao, Z. Ding, and M.-S. Alouini, "Multiple UAVs as relays: Multi-hop single link versus multiple dual-hop links," *IEEE Trans. Wireless Commun.*, vol. 17, no. 9, pp. 6348–6359, Sep. 2018.
- [11] M. Gapeyenko, V. Petrov, D. Moltchanov, S. Andreev, N. Himayat, and Y. Koucheryavy, "Flexible and reliable UAV-assisted backhaul operation in 5G mmWave cellular networks," *IEEE J. Sel. Areas Commun.*, vol. 36, no. 11, pp. 2486–2496, Nov. 2018.
- [12] B. Galkin, J. Kibilda, and L. A. DaSilva, "Backhaul for low-altitude UAVs in urban environments," in *Proc. IEEE Int. Conf. Commun.*, 2018, pp. 1–6.
- [13] N. Tafintsev et al., "Aerial access and backhaul in mmWave B5G systems: Performance dynamics and optimization," *IEEE Commun. Mag.*, vol. 58, no. 2, pp. 93–99, Feb. 2020.
- [14] W. Wang, N. Cheng, Y. Liu, H. Zhou, X. Lin, and X. Shen, "Content delivery analysis in cellular networks with aerial caching and mmwave backhaul," *IEEE Trans. Veh. Technol.*, vol. 70, no. 5, pp. 4809–4822, May 2021.
- [15] C. T. Cicek, H. Gultekin, B. Tavli, and H. Yanikomeroglu, "Backhaul-aware optimization of UAV base station location and bandwidth allocation for profit maximization," *IEEE Access*, vol. 8, pp. 154573–154588, 2020.
- [16] Z. Feng, L. Ji, Q. Zhang, and W. Li, "Spectrum management for MmWave enabled UAV swarm networks: Challenges and opportunities," *IEEE Commun. Mag.*, vol. 57, no. 1, pp. 146–153, Jan. 2019.
- [17] Y. Yu, X. Bu, K. Yang, H. Yang, and Z. Han, "UAV-aided low latency mobile edge computing with mmWave backhaul," in *Proc. IEEE Int. Conf. Commun.*, 2019, pp. 1–7.
- [18] A. Almohamad, M. O. Hasna, T. Khattab, and M. Haouari, "On network flow maximization via multihop backhauling and UAVs: An integer programming approach," in *Proc. IEEE 89th Veh. Technol. Conf.*, 2019, pp. 1–6.
- [19] M. Q. Vu, T. V. Pham, N. T. Dang, and A. T. Pham, "Outage performance of HAP-UAV FSO links with Gaussian beam and UAV hovering," in *Proc. IEEE 92nd Veh. Technol. Conf.*, 2020, pp. 1–5.
- [20] Y. Ma, J.-Y. Wang, J.-B. Wang, M. Lin, H. Zhang, and C. Chang, "Outage performance analysis and parameter optimization of hovering UAV-Based FSO system," in *Proc. IEEE Int. Conf. Commun.*, 2020, pp. 1–6.
- [21] H. S. Khallaf and M. Uysal, "UAV-based FSO communications for high speed train backhauling," in *Proc. IEEE Wireless Commun. Netw. Conf.*, 2019, pp. 1–6.
- [22] A. Kachroo et al., "Emulating UAV motion by utilizing robotic arm for mmWave wireless channel characterization," *IEEE Trans. Antennas Propag.*, vol. 69, no. 10, pp. 6691–6701, Oct. 2021.
- [23] M. T. Dabiri, M. Rezaee, V. Yazdani, B. Maham, W. Saad, and C. S. Hong, "3D channel characterization and performance analysis of UAV-assisted millimeter wave links," *IEEE Trans. Wireless Commun.*, vol. 20, no. 1, pp. 110–125, Jan. 2021.
- [24] M. T. Dabiri, M. O. Hasna, T. Khattab, and K. Qaraqe, "A study of multihop mmW aerial backhaul links," in *Proc. IEEE Int. Wireless Commun. Mobile Comput.*, 2022, pp. 1228–1233.
- [25] J. G. Proakis, *Digital Communications*, 5th ed. New York City, NY, USA: McGraw Hill, 2007.
- [26] International Telecommunication Union (ITU), "Attenuation by atmospheric gases," ITU, Geneva, Switzerland, Tech. Rep. ITU-R P.676-11, 2016.

- [27] 3rd Generation Partnership Project (3GPP), "Technical specification group radio access network; study of radio frequency (RF) and electromagnetic compatibility (EMC) requirements for active antenna array system (AAS) base station," 3GPP, Sophia Antipolis, France, Tech. Rep. 37.840 v12.1.0, 2013.
- [28] C. A. Balanis, *Antenna Theory: Analysis and Design*. Hoboken, NJ, USA: Wiley, 2016.
- [29] M. T. Dabiri, S. M. S. Sadough, and M. A. Khalighi, "Channel modeling and parameter optimization for hovering UAV-based free-space optical links," *IEEE J. Sel. Areas Commun.*, vol. 36, no. 9, pp. 2104–2113, Sep. 2018.
- [30] M. Nakamura, G. K. Tran, and K. Sakaguchi, "Interference management for millimeter-wave mesh backhaul networks," in *Proc. IEEE Annu. Consum. Commun. Netw. Conf.*, 2019, pp. 1–4.
- [31] S. Bhunia, P. A. Regis, and S. Sengupta, "Distributed adaptive beam nulling to survive against jamming in 3D UAV mesh networks," *Comput. Netw.*, vol. 137, pp. 83–97, 2018.
- [32] M. O. Hasna and M.-S. Alouini, "Outage probability of multihop transmission over Nakagami fading channels," *IEEE Commun. Lett.*, vol. 7, no. 5, pp. 216–218, May 2003.
- [33] A. Jeffrey and D. Zwillinger, *Table of Integrals, Series, and Products*. Amsterdam, The Netherlands: Elsevier, 2007.

ABDULLATEEF ALMOHAMAD (Graduate Student Member, IEEE) received the B.Sc. degree in communication engineering from the Higher Institute for Applied Sciences and Technology, Damascus, Syria, and the M.Sc. degree in electrical engineering. He is currently working toward the Ph.D. degree in electrical and computer engineering with Texas A&M university at Qatar, Ar-Rayyan, Qatar. He was an IP-Backbone Network Engineer with MTN Syria, Damascus, till 2017, before he joined Qatar University, Doha, Qatar, as a Research Assistant and a master's student in electrical engineering in 2018. He is also a frequent Reviewer in multiple IEEE conferences. His research interests include optimization, machine learning, aerial communications and backhauling, multiple access schemes, and reconfigurable intelligent surfaces. He received the Best Thesis Award for his M.Sc. degree.

MOHAMAD T. DABIRI received the Ph.D. degree (Hons.) in electrical engineering (telecommunications) from Shahid Beheshti University (SBU), Tehran, Iran, in 2018. From 2015 to 2018, he was the Research Assistant (Head of the Research Group) with the Optical Wireless Communications Laboratory, SBU. He is currently a Postdoctoral Fellow with the IRAN Telecommunication Research Center. His main research interests include wireless communications focusing on the design of compact and low weight optical and mmWave communication systems for unmanned aerial vehicles. He was the recipient of several awards, including the Exemplary accepted as the top Researcher at SBU in 2017 and 2018, Best Paper Award from the IEEE International Symposium on Communication Systems, Networks, and Digital Signal Processing in 2018, and Research Foundation Award from Iran National Science Foundation in 2019.

MAZEN O. HASNA (Senior Member, IEEE) received the B.S. degree in electrical engineering from Qatar University, Doha, Qatar, in 1994, the M.Sc. degree in electrical engineering from the University of Southern California, Los Angeles, CA, USA, in 1998, and the Ph.D. degree in electrical engineering from the University of Minnesota Twin Cities, Minneapolis, MN, USA, in 2003. In 2003, he joined the Staff of the Electrical Engineering Department, Qatar University, where he is currently a Professor of communications. From 2005 to 2017, he was with several administrative capacities within Qatar University, including the Head of Electrical Engineering Department, Dean of the College of Engineering, and VPCAO. He Co-founded and also serves on the Joint Management Committee with Qatar Mobility Innovation Center, an innovation center promoting using research and development to develop and deploy intelligent mobility and smart cities platforms and technologies. His research interests include the application of digital communication theory to the performance analysis of wireless communication systems, aerial networks, D2D enabled communications, physical layer security, FSO/RF hybrid networks, and RIS-based communications. He is listed in the 2015 Highly Cited Researchers List of Clarivate Analytics, and has received research grants in the last ten years worth of more than \$5M, both from industry and government. He is a Founding Member of the IEEE Qatar Section and was its founding VP. He is an Associate Editor for the IEEE WIRELESS COMMUNICATIONS LETTERS, *Frontiers in Communications and Networks*, and *Frontiers in Space Technologies*.

TAMER KHATTAB (Senior Member, IEEE) received the B.Sc. and M.Sc. degrees in electronics and communications engineering from Cairo University, Giza, Egypt, and the Ph.D. degree in electrical and computer engineering from The University of British Columbia (UBC), Vancouver, BC, Canada, in 2007. From 1994 to 1999, he was with IBM WTC, Giza, as a Development Team Member, and then as a Development Team Lead. From 2000 to 2003, he was with Nokia (formerly Alcatel Canada Inc.), Burnaby, BC, Canada, as a Senior Member of the Technical Staff. From 2006 to 2007, he was a Postdoctoral Fellow with The University of British Columbia, where he was involved in prototyping advanced Gbits/s wireless LAN baseband transceivers. He joined Qatar University (QU), Doha, Qatar, in 2007, where he is currently a Professor of electrical engineering. In addition to more than 150 high-profile academic journals and conference publications, he has several published and pending patents. His research interests include physical layer security techniques, information-theoretic aspects of communication systems, radar and RF sensing techniques, and optical communication. He is a Senior Member of the Technical Staff with Qatar Mobility Innovation Center, Research and Development Center owned by QU and funded by Qatar Science and Technology Park.

KHALID QARAQE (Senior Member, IEEE) was born in Bethlehem. He received the B.S. degree (Hons.) in electrical engineering from the University of Technology, Bagdad, Iraq, in 1986, the M.S. degree in electrical engineering from The University of Jordan, Amman, Jordan, in 1989, and the Ph.D. degree in electrical engineering from Texas A&M University, College Station, TX, USA, in 1997. From 1989 to 2004, he has held a variety positions in many companies and has more than 12 years of experience in the telecommunication industry. He joined the Department of Electrical and Computer Engineering, Texas A&M University at Qatar, Ar-Rayyan, Qatar, in July 2004, where he is currently a Professor and the Managing Director of the Center for Remote Healthcare Technology, Qatar. He has worked on numerous projects and has experience in product development, design, deployments, testing, and integration. He has authored or coauthored more than 131 journal articles in top IEEE journals, and has published and presented 250 papers at prestigious international conferences. He has 20 book chapters published, four books, three patents, and presented several tutorials and talks. His research interests include communication theory and its application to design and performance, analysis of cellular systems, and indoor communication systems, mobile networks, broadband wireless access, cooperative networks, cognitive radio, diversity techniques, index modulation, visible light communication, FSO, tele-health, and noninvasive bio sensors. He has been awarded more than 20 research projects consisting of more than USD 13M from local industries in Qatar and the Qatar National Research Foundation.